Electronic Supplementary Material (ESI) for Journal of Materials Chemistry C.

The *σ−π* and *p−π* Conjugation Induced NIR-Emitting Iridium(III) Complexes by Anchoring Flexible Side Chains in Rigid Dibenzo [a,c]phenazine Moiety and Their Application in High-Efficient Solution-Processable NIR-Emitting Devices

Caifa You[a], Denghui Liu[b], Mengbing Zhu[b], Junting Yu[b], Bin Zhang[b], Yu Liu[b], Yafei Wang[b], Weiguo Zhu*[a, b]

[a] *College of Chemistry, Key Lab of Environment-Friendly Chemistry and Application in the Ministry of Education, Xiangtan University, Xiangtan 411105, China.*

[b] *School of Materials Science and Engineering, Jiangsu Collaboration Innovation Center of Photovoltaic Science and Engineering, Jiangsu Engineering Laboratory of Light-Electricity-Heat Energy-Converting Materials and Applications, National Experimental Demonstration Center for Materials Science and Engineering,*

Changzhou University, Changzhou 213164, P. R. China.

Table of Contents

1. Experimental Section

1.1. Materials and methods

All reagents and chemicals were purchased from commercial sources and used directly without further purification. The toluene and dichloromethane were distilled according to the common methods. All manipulations of air and water sensitive compounds were carried out under dry N_2 using the standard Schlenk line techniques. Column chromatography was carried out with Merck silica gel (200–300 mesh). All reactions were performed under a nitrogen atmosphere to avoid the oxidation of the reactants by oxygen. Thin-layer chromatography (TLC) with Merck pre-coated was adopted to monitor reactions until the reactants were consumed completely.

^{1}H-NMR spectra were recorded at room temperature on Bruker Avance III 400 and 500 MHz NMR (100 or 126 MHz for ^{13}C-NMR) spectrometer and the chemical shifts (δ) are reported in parts per million (ppm) using tetramethyl silane (TMS) signals as internal standards. Matrix-assisted laser desorption ionization time of flight mass spectrometry (MALDI-TOF-MS) was performed with Bruker Daltonics AutoflexTM III using α-cyano-4- hydroxycinnamic acid (CCA) as a matrix. Elemental analysis was measured with Vario EL III elementary analyzer. Single-crystal X-ray diffraction data were recorded on a Bruker SMART APEX II CCD diffractometer using λ (Cu Kα) radiation (λ=1.34139 Å). Cyclic voltammetry (CV) was performed using CHI630E at a scan rate of 100 mV s^{-1}. All experiments were carried out in a three-electrode compartment cell with a Pt-wire counter electrode, a Pt-disk working electrode and Ag/AgCl reference electrode. The supporting electrolyte used was 0.1 M tetrabutylammonium hexafluorophosphate ($[Bu_4N]PF_6$) solution in dry acetonitrile under a nitrogen atmosphere using ferrocene (Fc) as the calibrant. The potential of Fc/Fc^{+} *vs* Ag/AgCl electrode was measured to be 0.43 V. The highest occupied molecular orbital (HOMO) and the lowest unoccupied molecular orbital (LUMO) energy levels of each complex are calculated according to the following equations,[1] $E_{\mathrm{HOMO}} = -(E_{[\mathrm{onset,\ ox}\ vs\ \mathrm{Fc}^{+}/\mathrm{Fc}]} + 4.8)$ eV, $E_{\mathrm{LUMO}} = -(E_{[\mathrm{onset,\ red}\ vs\ \mathrm{Fc}^{+}/\mathrm{Fc}]} + 4.8)$ eV. The thermal gravimetric analysis (TGA) was performed on a TA Instruments (TGA 50) under nitrogen gas flow with a heating rate of 10 ^{o}C min^{-1}.

UV-Vis absorption spectra were carried out on Cary 100 spectrophotometer. Steady-state fluorescence measurements were recorded on Shimadzu UV-2600, while time-resolved fluorescence measurements and phosphorescence at 77 K was measured on Edinburgh Instruments (FLS980). The photoluminescence quantum yields (PLQYs) of iridium complex were measured in degassed CH_2Cl_2 solutions in accordance with $Ir(DBQ)_2(acac)$ as standard (Φ_P=0.53, in CH_2Cl_2 solution at 298 K, λ_{ex}=370 nm).[2] PLQYs was calculated using the equation of $\Phi_s=\Phi_r(\eta_s^2 I_S A_r/\eta_r^2 I_r A_s)$, where Φ stands for the quantum yield, η is the refractive index of the solvent, A is the absorbance of the sample or the reference at the wavelength of excitation, and I presents the integrated areas of emission bands, subscript ''s" and ''r" represents sample and reference, respectively.[3]

1.2. Preparation of NIR-emitting devices

The device structures of NIR-PLEDs and NIR-OLEDs are ITO/PEDOT: PSS (40 nm) /poly-TPD (30 nm)/[(PVK: OXD-7)7:3]: dopants (X wt%, 80 nm)/TmPyPB (50 nm)/CsF (1.2 nm)/Al (120 nm) and ITO/PEDOT: PSS (40 nm) /CBP: dopants (X wt%, 55-60 nm)/TmPyPB (50 nm)/CsF (1.2 nm)/Al (120 nm), respectively. In these made devices, PEDOT: PSS and poly-TPD are acted as hole-injection layer (HIL) and hole-transporting layer (HTL), respectively. PVK: OXD-7 and CBP are served as carrier transporting materials. X represents the doping ratio of iridium complexes into PVK: OXD-7 and CBP. TmPyPB is served as an electron-transporting layer (ETL) and hole-blocking layer (HBL). CsF is used as an electron-injection layer (EIL) and Al is acted as a cathode. PEDOT: PSS films covered by poly-TPD (30 nm), are spin coated on precleaned ITO glass substrates and annealed at 150 °C for 15 min (thickness: 40 nm). Subsequently, the blend of PVK: OXD-7 and dopants in chlorobenzene solution is spin coated on top of the poly-TPD (thickness: 80 nm). In the optimized NIR-OLEDs, the blend of CBP and dopants in chlorobenzene solution is spin coated on top of PEDOT: PSS films and annealed at 60 ^{o}C for 15 min. Finally, 50 nm of TmPyPB, 1.2 nm of CsF, and 120 nm of aluminum are evaporated with a shadow mask at pressure of 2×10^{-5} Pa. The thickness of the evaporated ETL and cathode is monitored by a quartz crystal thickness monitor (Model: STM-100/MF, Sycon). The active area of the OLEDs was 4 mm^2. To avoid degradation and emission quenching because of oxygen and moisture, these PLEDs were encapsulated in a glove box prior to the device characterization.

1.3. Measurements of NIR-emitting devices

The EL spectra and current density (*J*)-voltage (*V*)-luminance (*L*) curves are obtained using a PHOTO RESEARCH Spectra Scan PR 735 photometer and a KEITHLEY 2400 Source Meter constant current source at room temperature. The EQE values are measured by calculation assuming a Lambertian distribution.

1.4. Synthesis

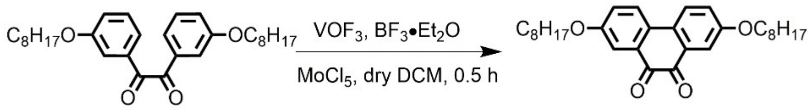

2

Scheme S1. Synthetic procedure for the intermediate **2**.

Synthesis of intermediate 2: Synthetic procedure followed the reported literatures by modified process.[4, 5] To a solution of 1,2-bis(3-(octyloxy)phenyl)ethane-1,2-dione (1.0 g，2.1 mmol)in dry CH_2Cl_2 was added $BF_3{\cdot}EtO_2$ (0.36 mL) solution and VOF_3 (0.58 g, 4.7 mmol) at 0 ^oC under nitrogen atmosphere and the resulting mixture was stirred for 5 min. $MoCl_5$ (1.3 g, 4.8 mmol) was added and the mixture was stirred for 30 min at room temperature, and then a 10% $NaHCO_3$ (50 mL) was added. The organic phase was separated, and the aqueous phase was extracted with CH_2Cl_2. The combined organic phase was washed with H_2O, dried over anhydrous $MgSO_4$, and evaporated under reduced pressure. The residue was purified by silica gel column chromatography (petroleum ether/ dichloromethane = 1/1 (*V/V*) as the eluent) to afford **2** as a deeply red solid (yield 75%). ^1H NMR (400 MHz, $CDCl_3$) δ (ppm): 7.75 (d, J = 8.8 Hz, 2H), 7.56 (d, J = 2.8 Hz, 2H), 7.19 (dd, J = 8.8, 2.9 Hz, 2H), 4.04 (t, J = 6.6 Hz, 4H), 1.87 – 1.75 (m, 4H), 1.51 – 1.42 (m, 4H), 1.33 (dd, J = 14.1, 8.5 Hz, 16H), 0.89 (t, J = 6.8 Hz, 6H).

^{13}C NMR (126 MHz, $CDCl_3$) δ (ppm): 180.54, 159.44, 131.20, 129.51, 125.15, 124.38, 113.39, 112.97, 68.70, 31.94, 29.46, 29.36, 29.23, 26.10, 22.80, 14.24.

General synthesis procedure for Schiff-base condensation reaction: A mixture of compound **1** or **2**, and one equivalent o-phenylenediamine in absolute ethanol with catalytical amount of acetic acid was heated to reflux for 4 h under vigorous stirring. A large amount of solid was obtained after filtration. It was further purified with a flash silica gel column using petroleum ether/dichloromethane mixture as the eluent to give the desired product.

L-R: The crude product was purified by silica column chromatography (petroleum ether: dichloromethane = 10/1 (*V/V*) as the eluent) to give white solid in a yield of 90%. ^{1}H NMR (400 MHz, $CDCl_3$) δ (ppm): 9.17 (d, J = 1.7 Hz, 2H), 8.42 (d, J = 8.3 Hz, 2H), 8.38 – 8.31 (m, 2H), 7.88 – 7.80 (m, 2H), 7.60 (dd, J = 8.3, 1.9 Hz, 2H), 2.98 – 2.86 (m, 4H), 1.81 (m, 4H), 1.47 – 1.25 (m, 20H), 0.88 (t, J = 6.8 Hz, 6H). ^{13}C NMR (125 MHz, $CDCl_3$) δ (ppm): 142.92, 142.69, 142.17, 131.11, 130.26, 129.98, 129.67, 129.54, 125.61, 122.87, 36.26, 32.06, 31.79, 29.70, 29.68, 29.46, 22.84, 14.27. MS (MALDI-TOF) *m/z*: $[M+H]^+$ calcd for $C_{36}H_{45}N_2$: 505.350; found, 505.310. Anal. Calcd for $C_{36}H_{44}N_2$: C, 85.66; H, 8.79; N, 5.55. found: C, 85.58; H, 8.89; N, 5.61.

L-OR: The crude product was purified by silica column chromatography (petroleum ether/ dichloromethane = 3/1 (*V/V*) as the eluent) to yellow-green solid in a yield of 85%. ^{1}H NMR (400 MHz, $CDCl_3$) δ (ppm): 8.82 (d, J = 2.5 Hz, 2H), 8.36 (dd, J = 9.5, 3.7 Hz, 4H), 7.86 (dd, J = 6.5, 3.4 Hz, 2H), 7.36 (dd, J = 8.8, 2.5 Hz, 2H), 4.29 (t, J = 6.5 Hz, 4H), 1.98 – 1.85 (m, 4H), 1.64 – 1.57 (m, 4H), 1.50 – 1.26 (m, 16H), 0.91 (t, J = 6.5 Hz, 6H). ^{13}C NMR (125 MHz, $CDCl_3$) δ (ppm): 158.38, 142.60, 142.06, 130.64, 129.62, 129.53, 125.99, 123.96, 119.84, 108.33, 68.45, 32.02, 29.63, 29.57, 29.47, 26.34, 22.85, 14.28. MS (MALDI-TOF) *m/z*: $[M+H]^+$ calcd for $C_{36}H_{45}N_2O_2$: 537.340; found, 537.388. Anal. Calcd for $C_{36}H_{44}N_2O_2$: C, 80.56; H, 8.26; N, 5.22. found: C, 81.24; H, 8.19; N, 5.28.

General synthesis procedure for iridium(III) μ-chloro-dimer complexes. Under N_2 atmosphere, one eq. of $[Ir^{I}(Cl)(COD)]_2$ and four equivalents of ligand **L-R** or **L-OR** were heated to 115 ^{o}C and stirred for 24 h in 20 mL fresh-distilled toluene. The reaction mixture slowly turned to dark black. Toluene was removed under reduced pressure. Without further purification, the crude product was used for the next reaction.

2. Supplementary Figures and Tables

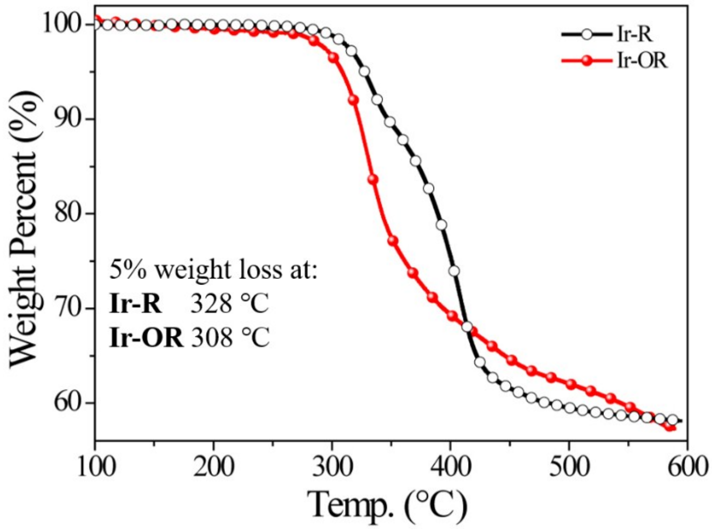

Fig. S1 TGA curves of **Ir-R** and **Ir-OR** under N_2 atmosphere.

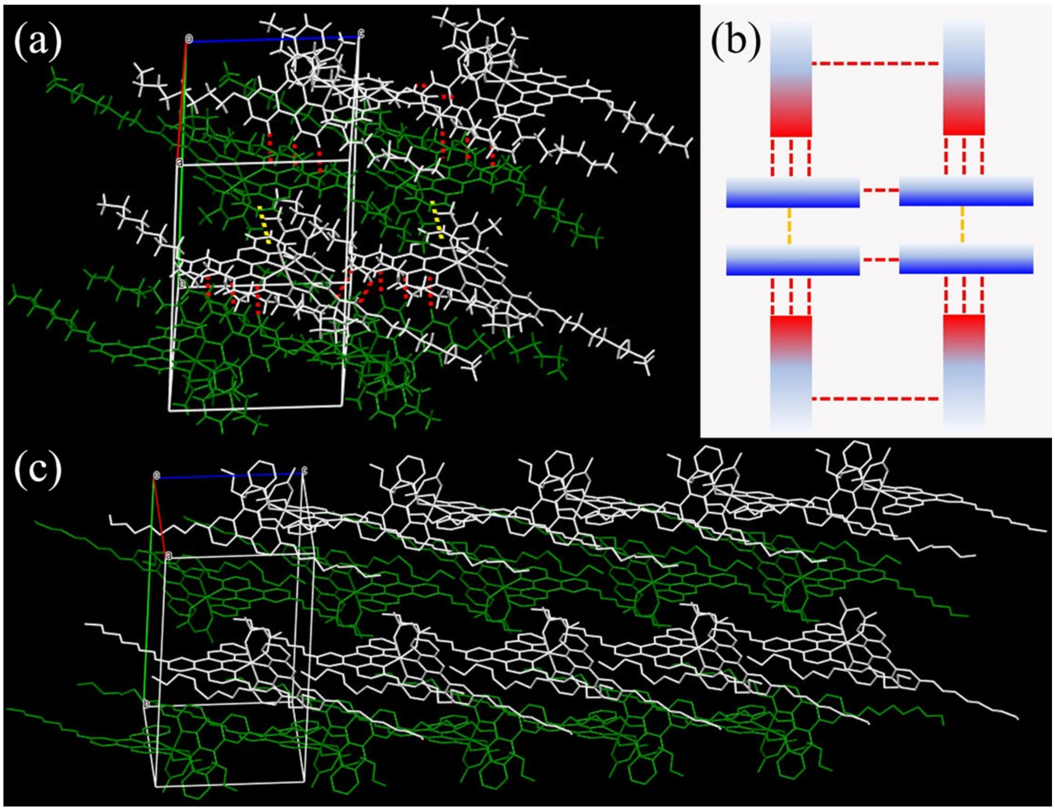

Fig. S2 (a) Molecular packing mode of complex **Ir-OR** along c axis, red dashed lines and yellow dashed lines present C-H···π and π-π interactions, respectively. (b) Simplified schematic diagram of complex **Ir-OR**; (c) packing diagram of complex **Ir-OR** without hydrogen atoms to understand more clearly.

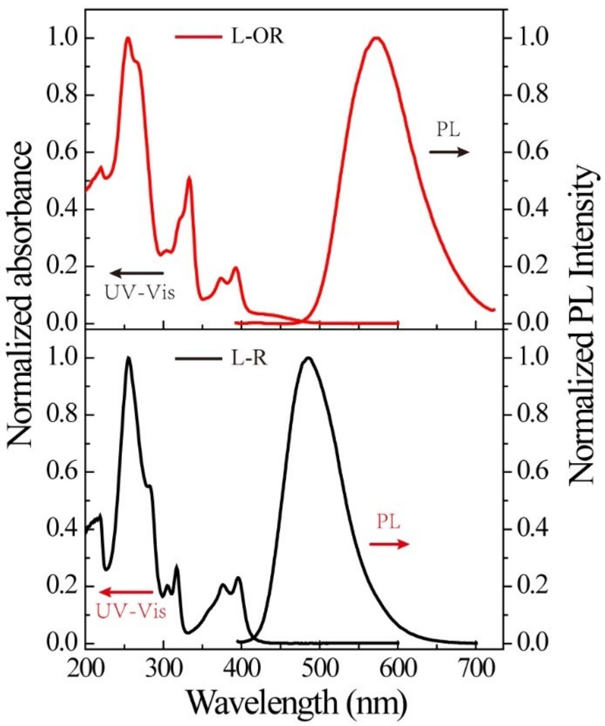

Fig. S3 Absorption and emission spectra of C^N ligands **L-R** and **L-OR** in 1×10^{-5} M DCM at RT, Ex = 375 and 373 nm for **L-R** and **L-OR**, respectively.

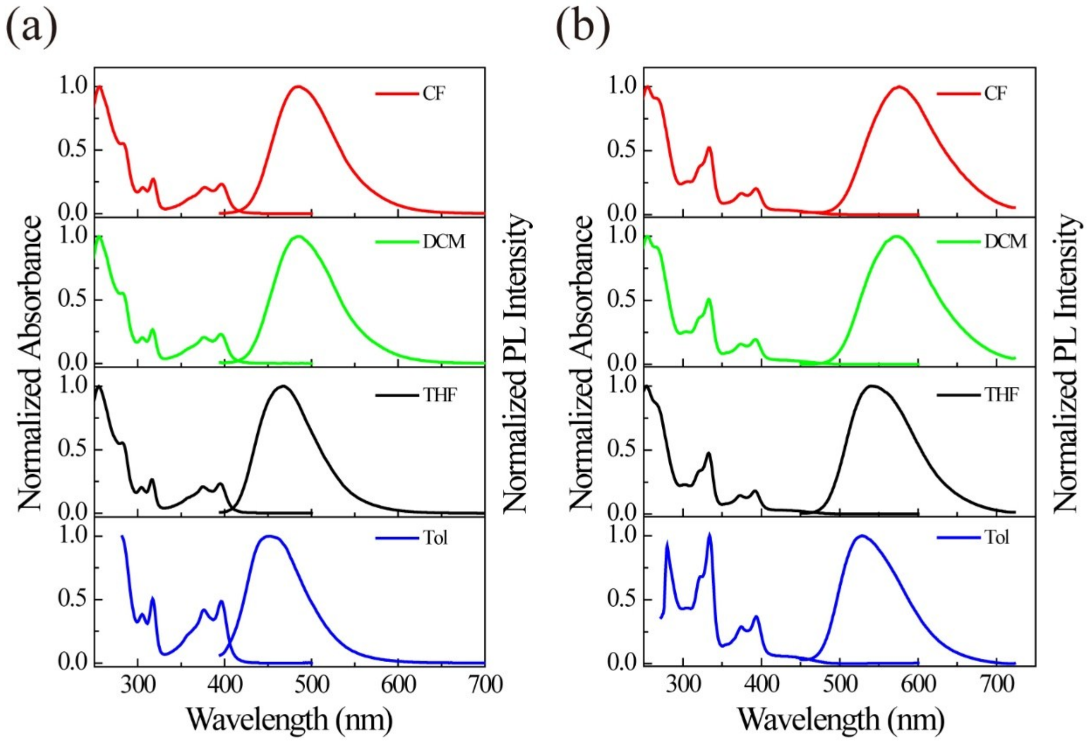

Fig. S4 UV-Vis and PL Spectra of C^N ligands **L-R** (a) and **L-OR** (b) in different solvents under the same measurement conditions, Ex = 375 and 373 nm for **L-R** and **L-**

OR, respectively.

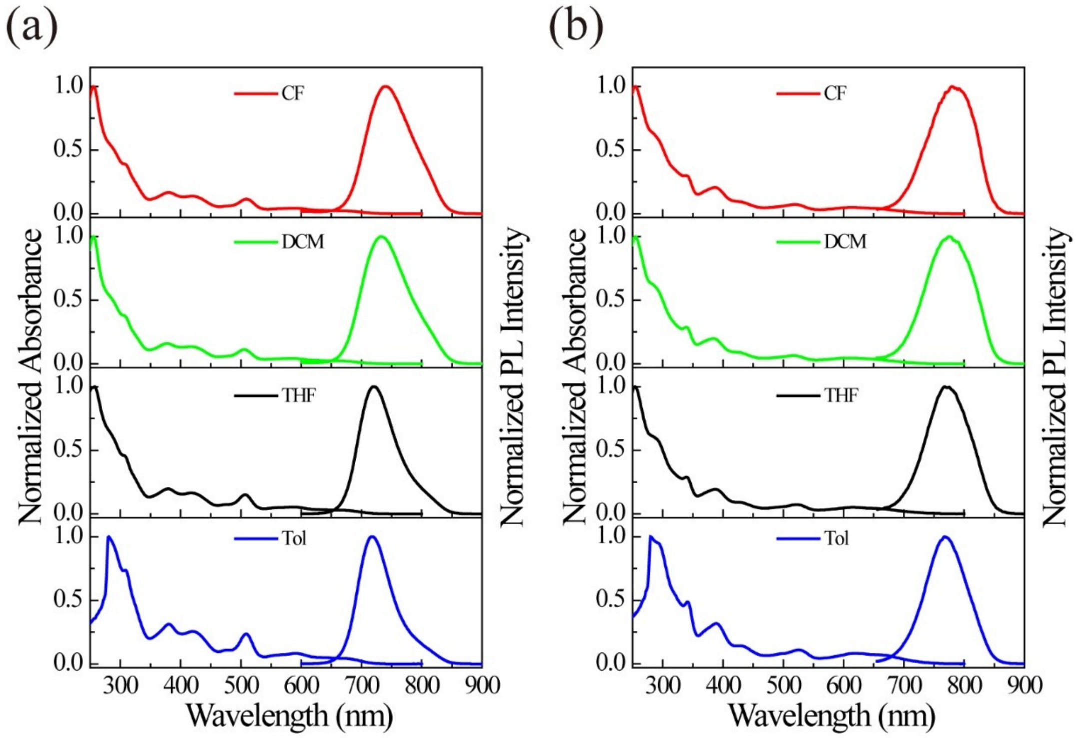

Fig. S5 Absorption and emission spectra of complexes **Ir-R** (a) and **Ir-OR** (b) at RT in different solvents under same measurement conditions, Ex = 500 nm, and 510 nm for **Ir-R** and **Ir-OR** respectively.

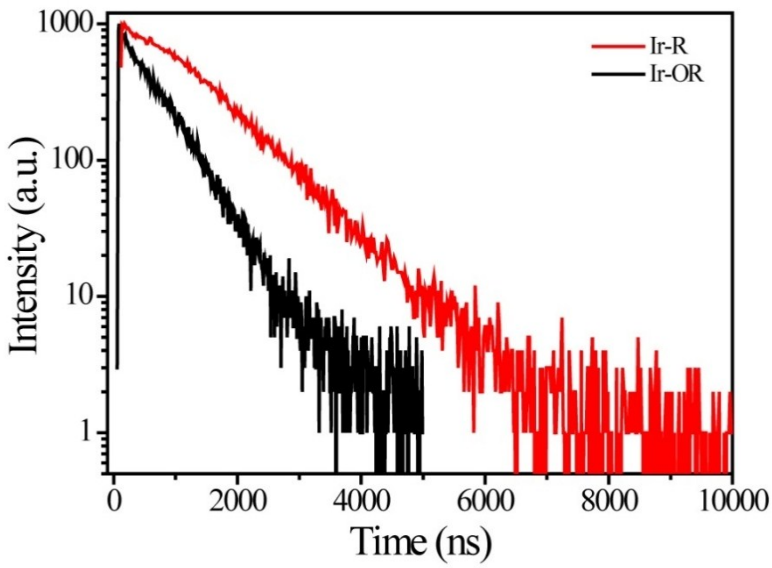

Fig. S6 Transient PL decay curves of complex **Ir-R** and **Ir-OR** in degassed DCM solution (1×10^{-5} M) at RT.

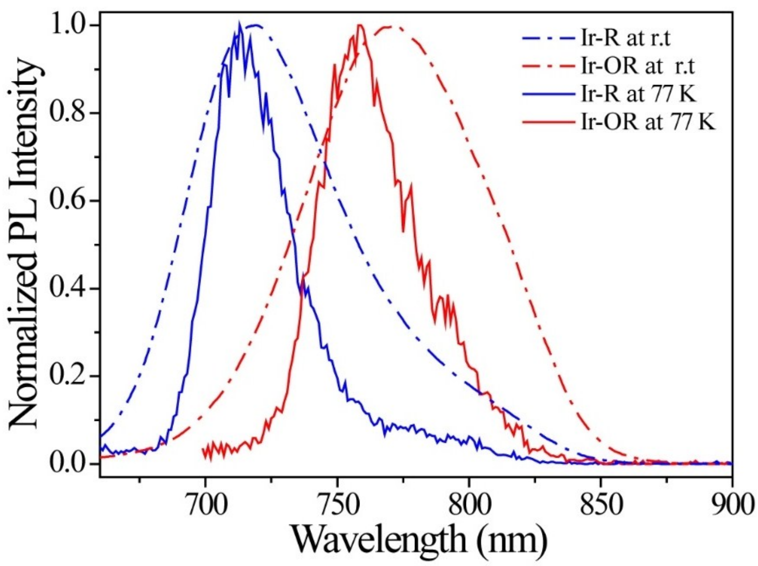

Fig. S7 Normalized emission spectra of the two Ir(III) complexes in dilute 2-MeTHF (1×10^{-5} M) at 77 K compared with the emission spectra at RT.

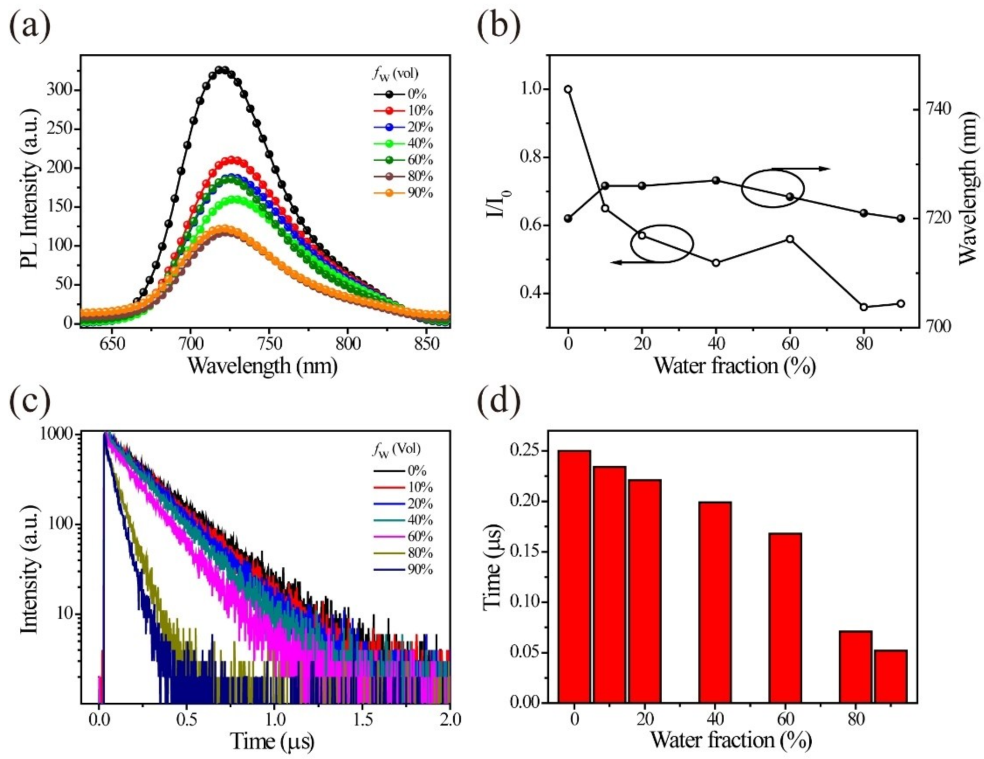

Fig. S8 PL spectra of **Ir-R** in THF/H_2O mixtures with different water fractions with a concentration of 10^{-5} M at 298 K, Ex = 500 nm (a); relationships between the ratio of I/I_0 and the emission maximum *versus* water fraction in THF/H_2O mixtures (b), I_0 stands for the emission intensity in pure THF while I means emission intensity in THF/H_2O mixtures; PL decay spectra of **Ir-R** in THF/H_2O mixtures with different water fractions (c); lifetimes *versus* water fractions in THF/H_2O mixtures (d).

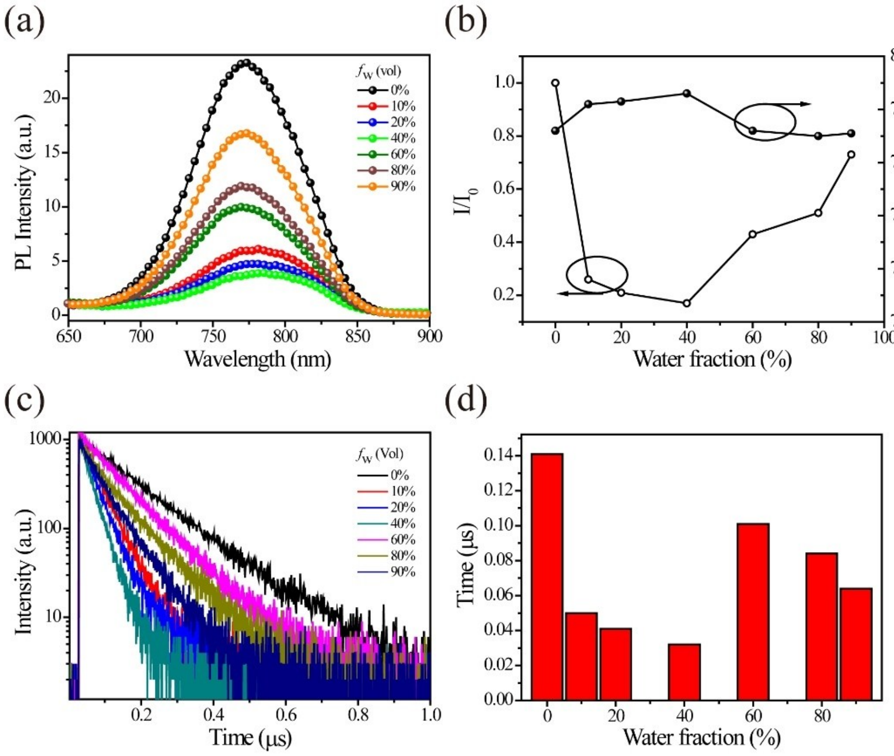

Fig. S9 PL spectra of **Ir-OR** in THF/H_2O mixtures with different water fractions with a concentration of 10^{-5} M at 298 K, Ex = 510 nm (a); relationships between the ratio of I/I_0 and the emission maximum *versus* water fraction in THF/H_2O mixtures (b), I_0 stands for the emission intensity in pure THF while I means emission intensity in THF/H_2O mixtures; PL decay spectra of **Ir-OR** in THF/H_2O mixtures with different water fractions (c); lifetimes *versus* water fractions in THF/H_2O mixtures (d).

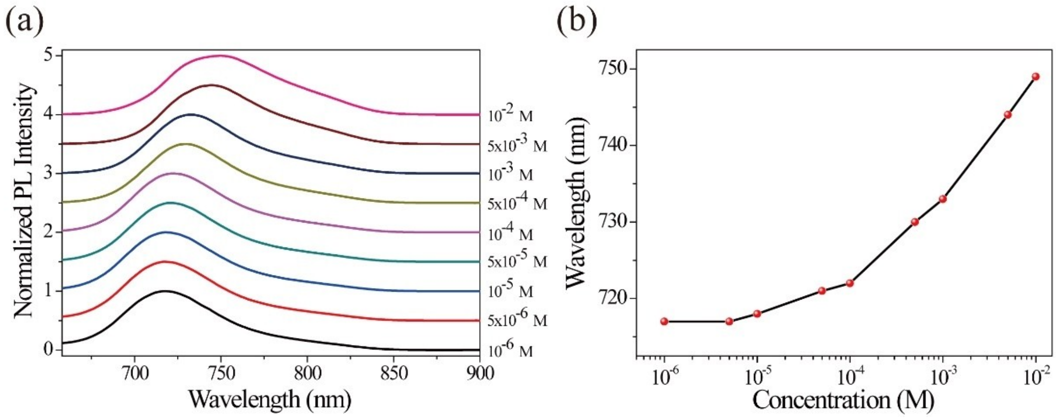

Fig. S10 PL spectra of **Ir-R** in different concentrations of toluene (a), Ex = 500 nm, and the plot of emission maximum *versus* the concentration of the solution (b).

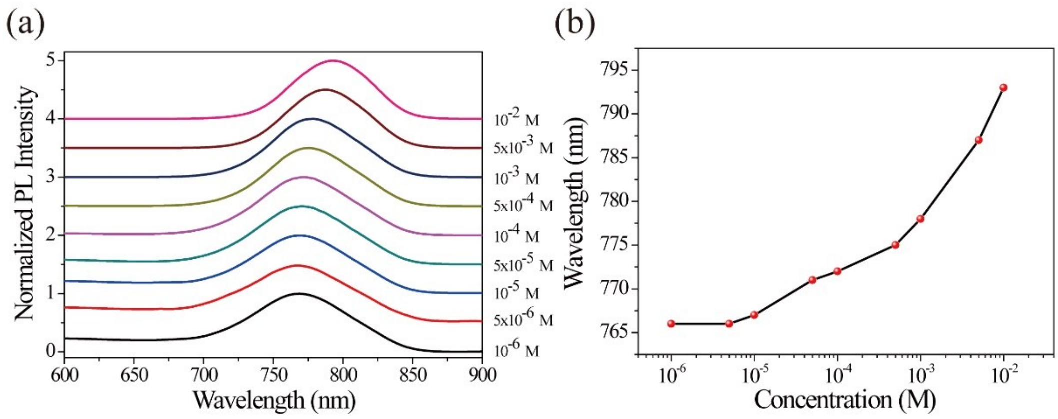

Fig. 11 PL spectra of **Ir-OR** in different concentrations of toluene (a), Ex = 510 nm, and the plot of emission maximum *versus* the concentration of the solution (b).

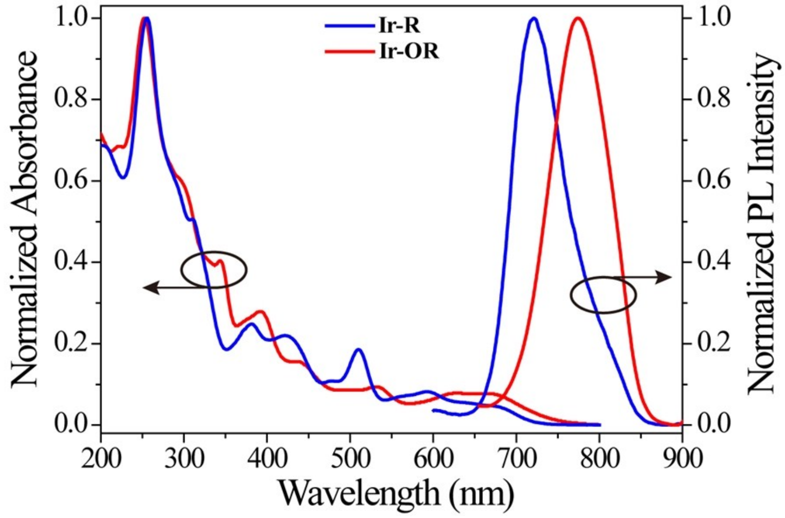

Fig. S12 UV-Vis and PL spectra of complexes **Ir-R** and **Ir-OR** in neat films, Ex = 500 nm, 510 nm for **Ir-R** and **Ir-OR** respectively.

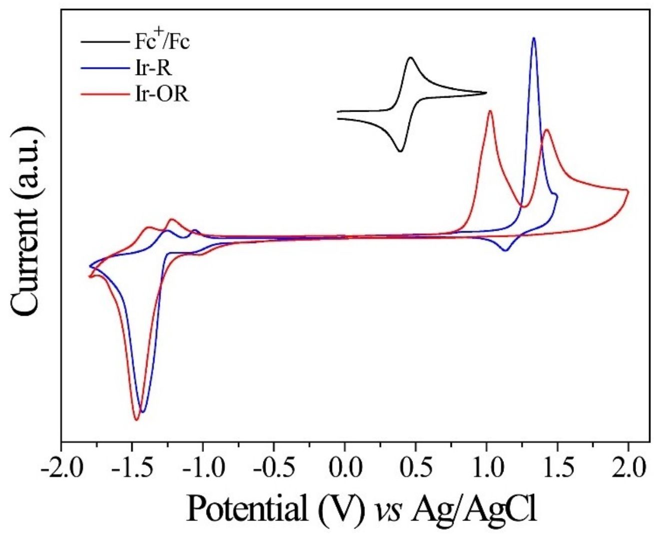

Fig. S13 Cyclic voltammograms of **Ir-R** and **Ir-OR** in CH_3CN.

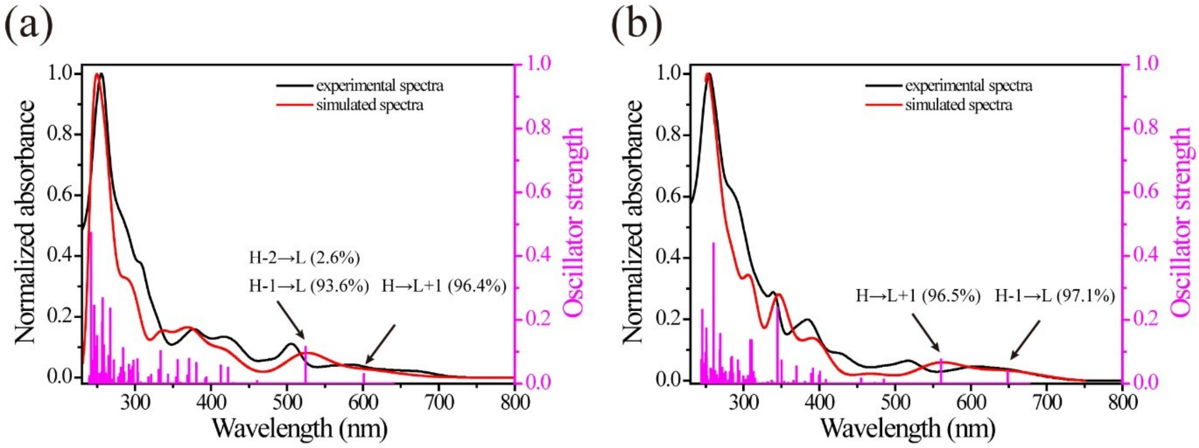

Fig. S14 Experimental UV−Vis absorption spectra (red profile) and simulated spectra (black profile) with discrete vertical vibronic transitions for these two iridium(III) complexes.

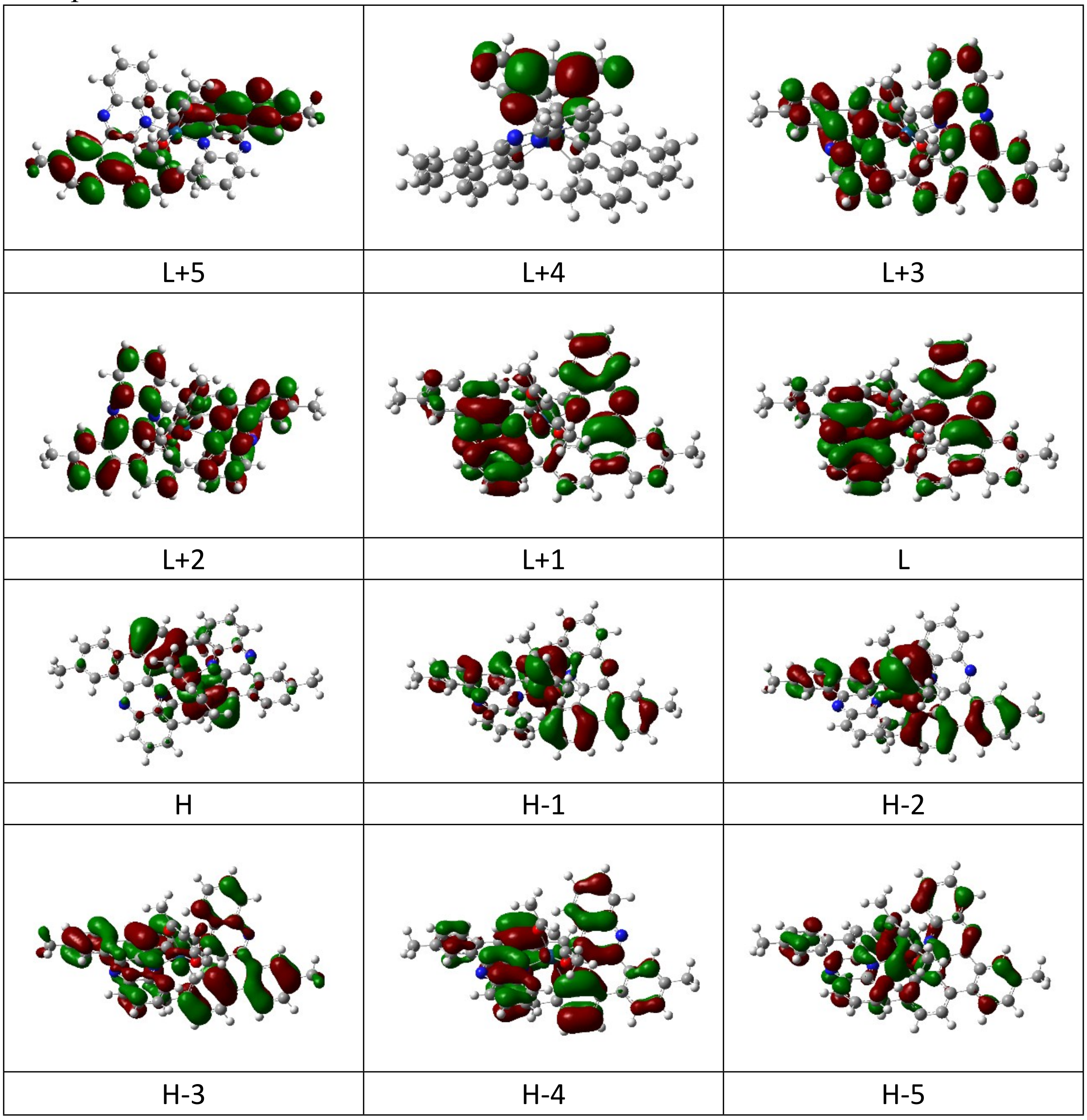

Fig. S15 Selected molecular orbital diagrams of complex **Ir-R** based on its optimized triplet state geometry.

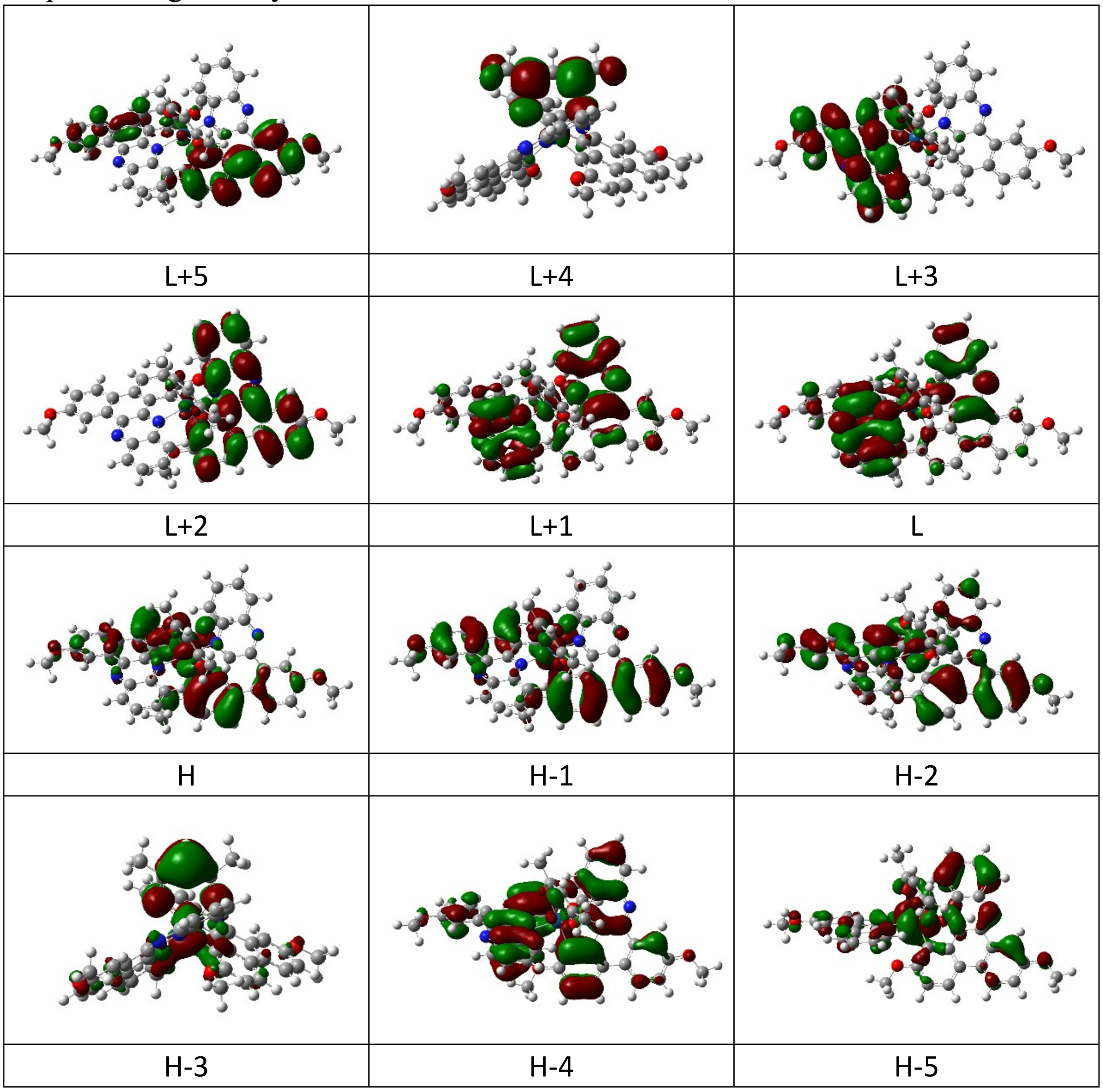

Fig. S16 Selected molecular orbital diagrams of complex **Ir-OR** based on its optimized triplet state geometry.

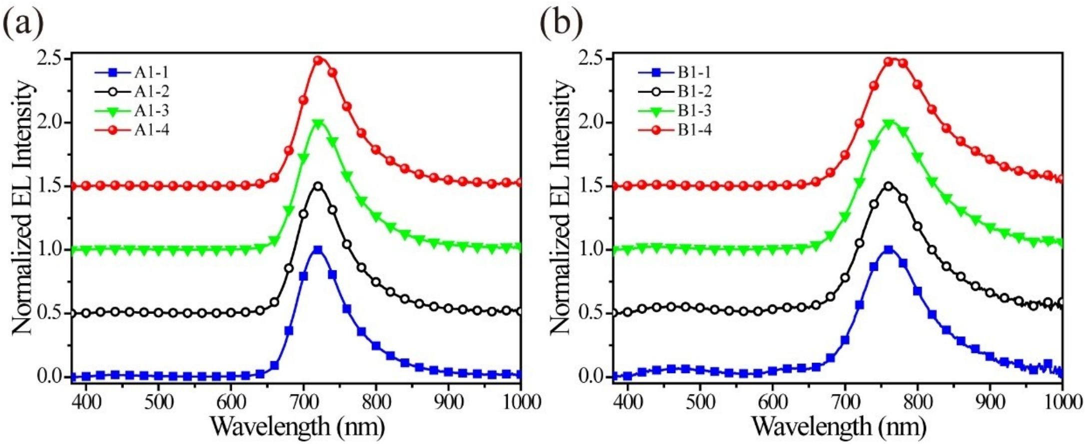

Fig. S17 Normalized EL spectra of device A1 (a) and B1 (b).

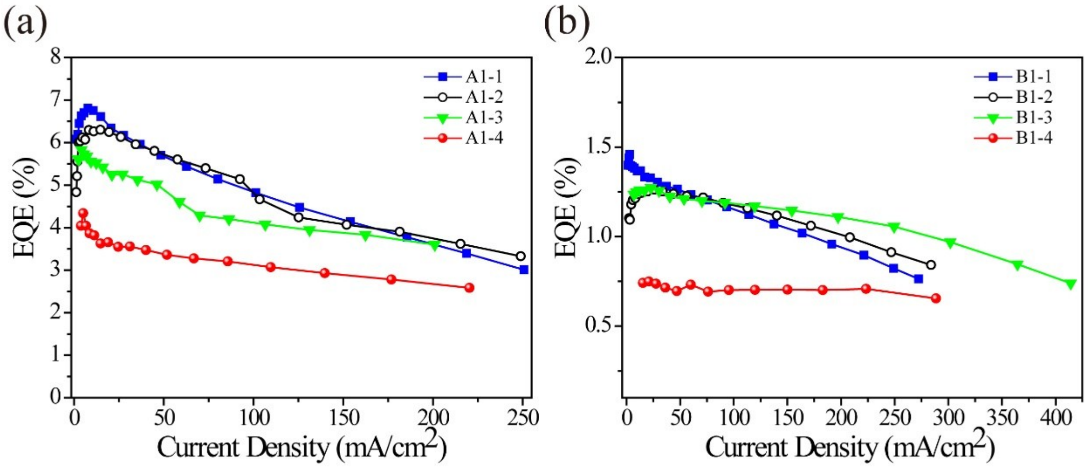

Fig. S18 EQE-*J* characteristics of device A1 (a) and B1 (b).

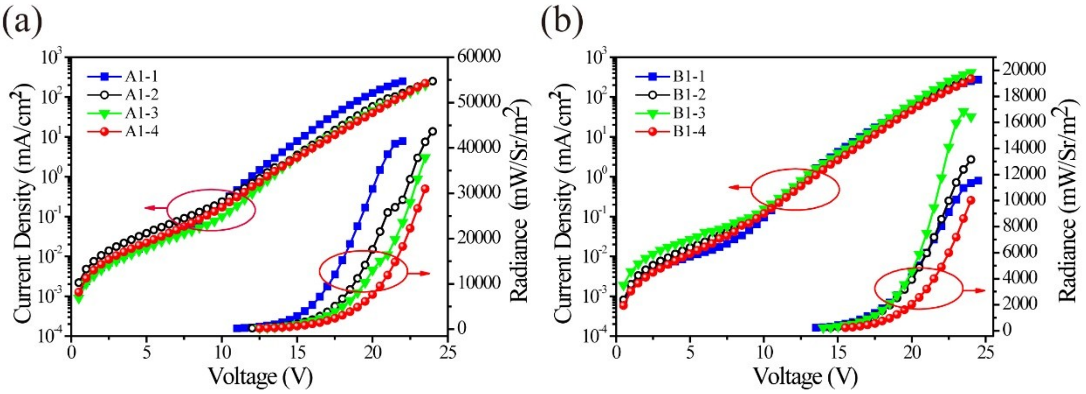

Fig. S19 *J*-*V*-*R* profiles of device A1 (a) and B1 (b).

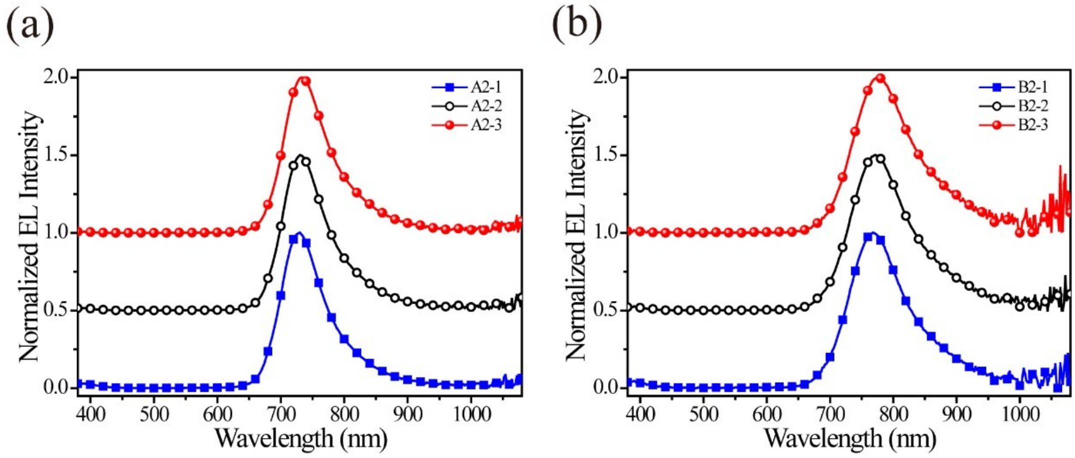

Fig. S20 Normalized EL spectra of device A2 (a) and B2 (b).

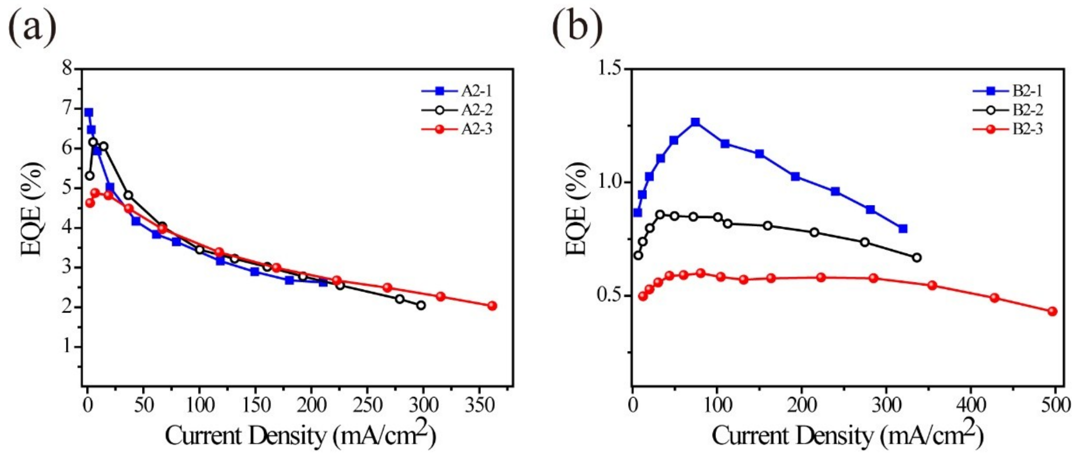

Fig. S21 EQE-*J* characteristics of device A2 (a) and B2 (b).

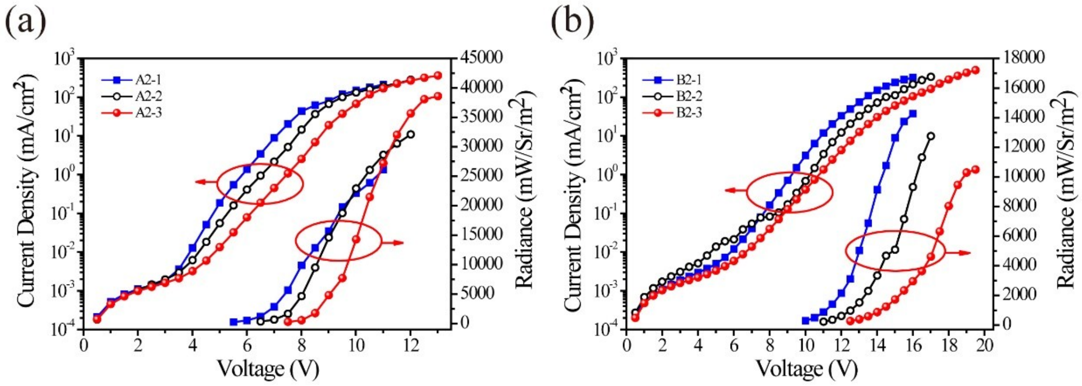

Fig. S22 *J-V-R* profiles of device A2 (a) and B2 (b).

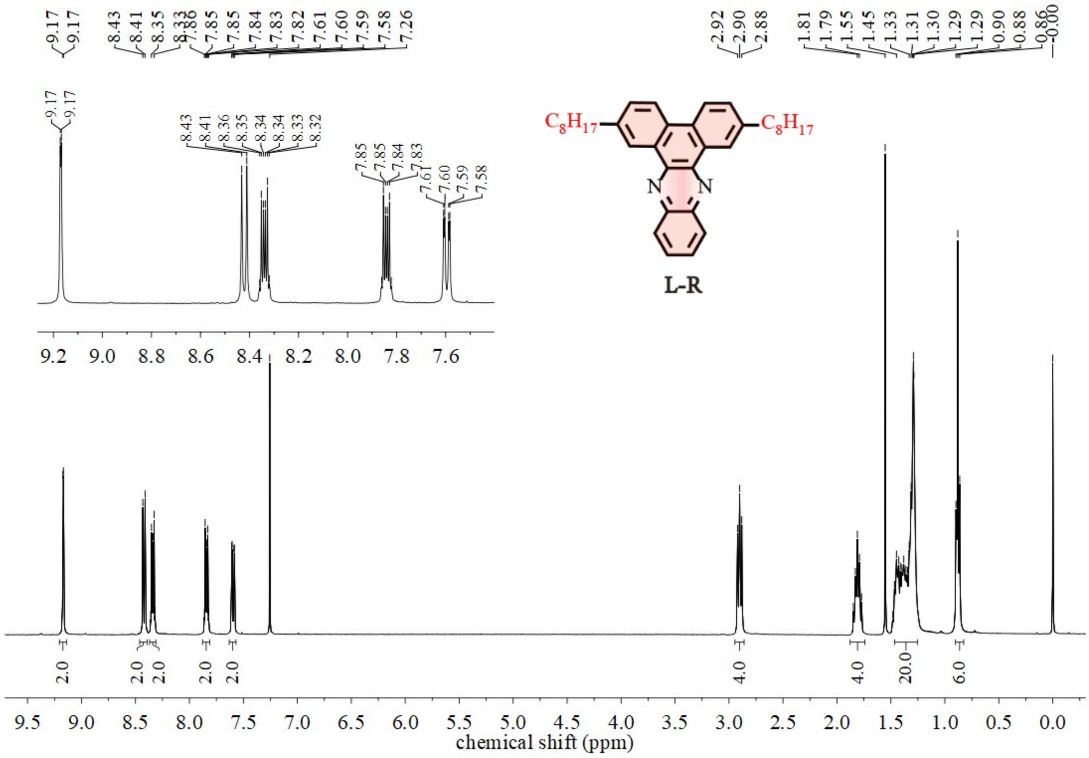

Fig. S23 ^{1}H-NMR spectrum of C^N ligand **L-R** (400 MHz, $CDCl_3$, r.t).

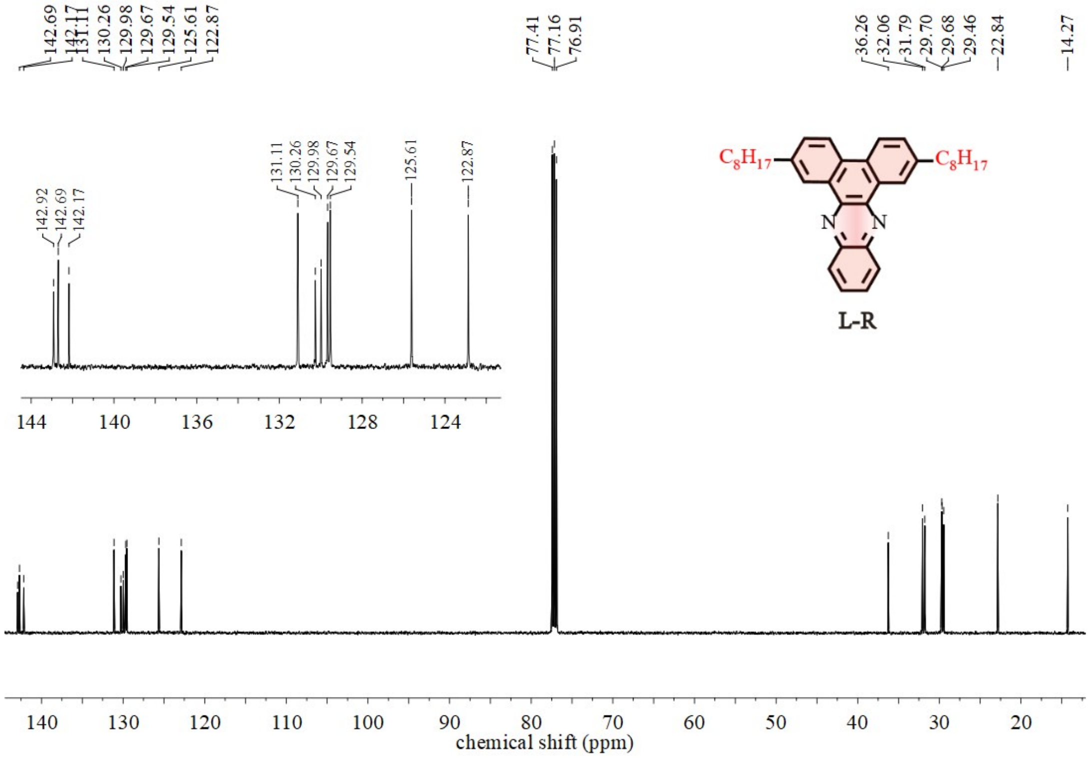

Fig. S24 ^{13}C-NMR of C^N ligand **L-R** (126 MHz, $CDCl_3$, r.t).

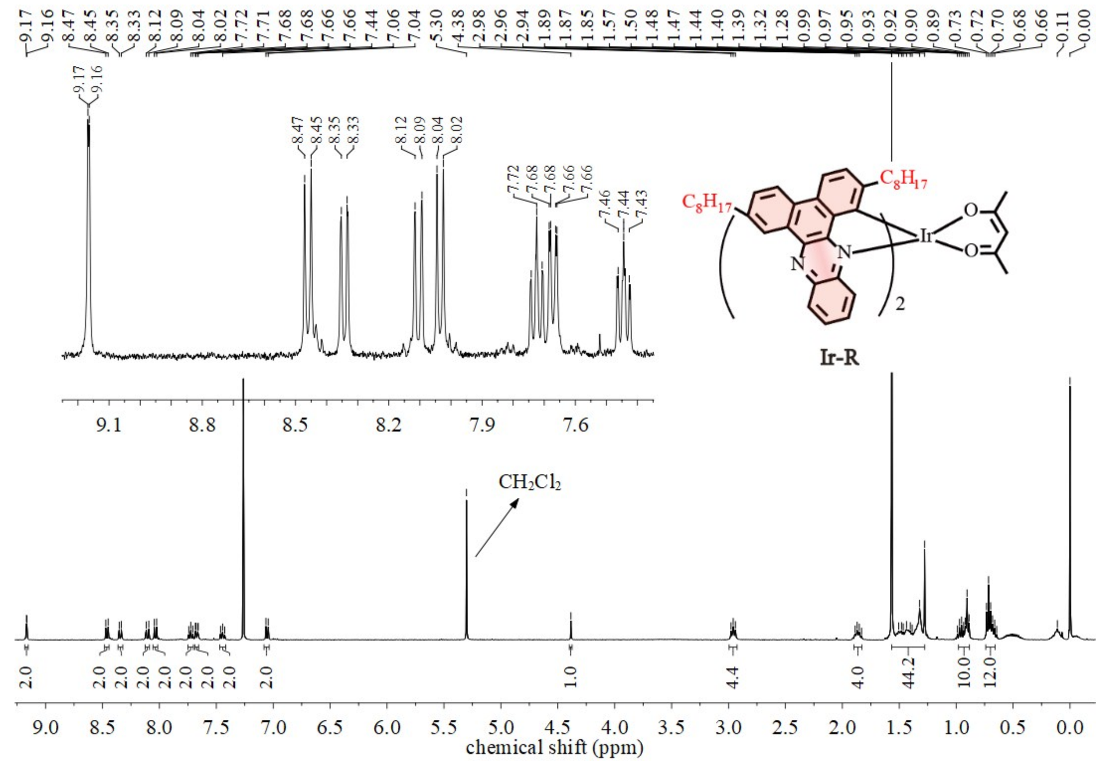

Fig. S25 ^{1}H-NMR of complex **Ir-R** (400 MHz, $CDCl_3$, r.t).

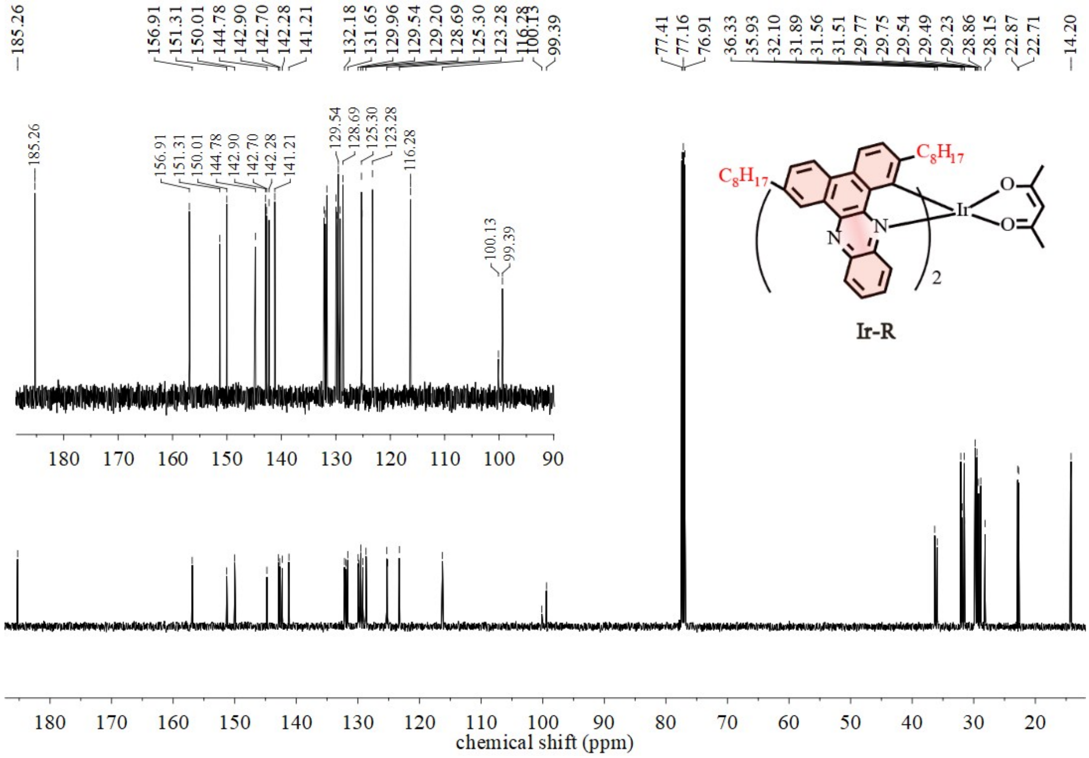

Fig. S26 ^{13}C-NMR of complex **Ir-R** (126 MHz, $CDCl_3$, r.t).

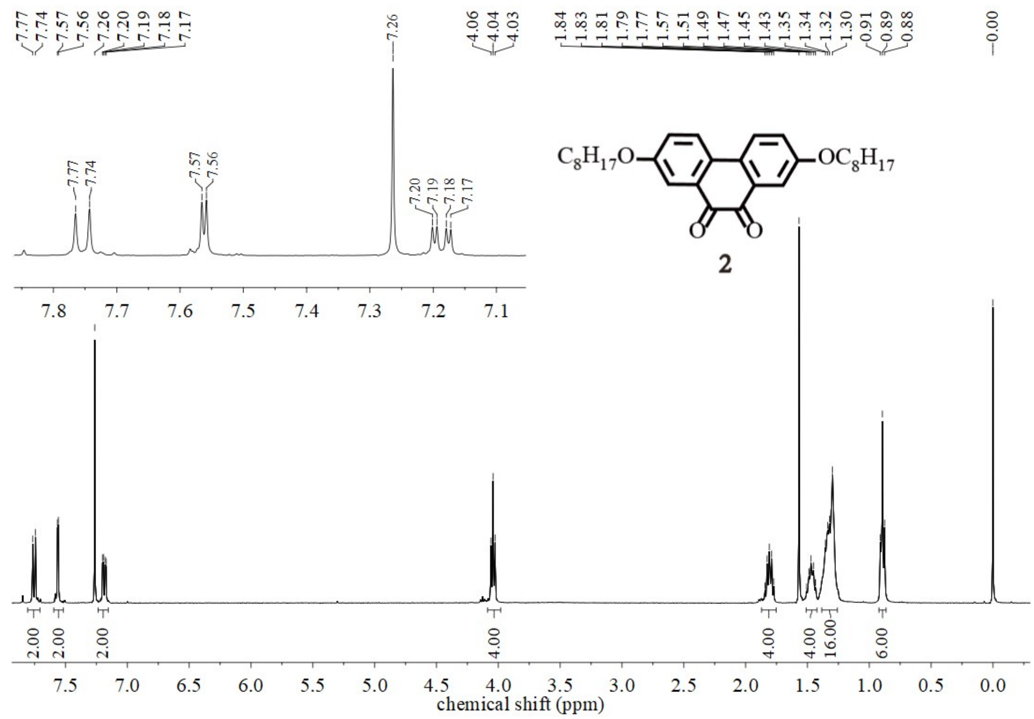

Fig. S27 ^{1}H-NMR of intermediate compound **2** (400 MHz, $CDCl_3$, r.t).

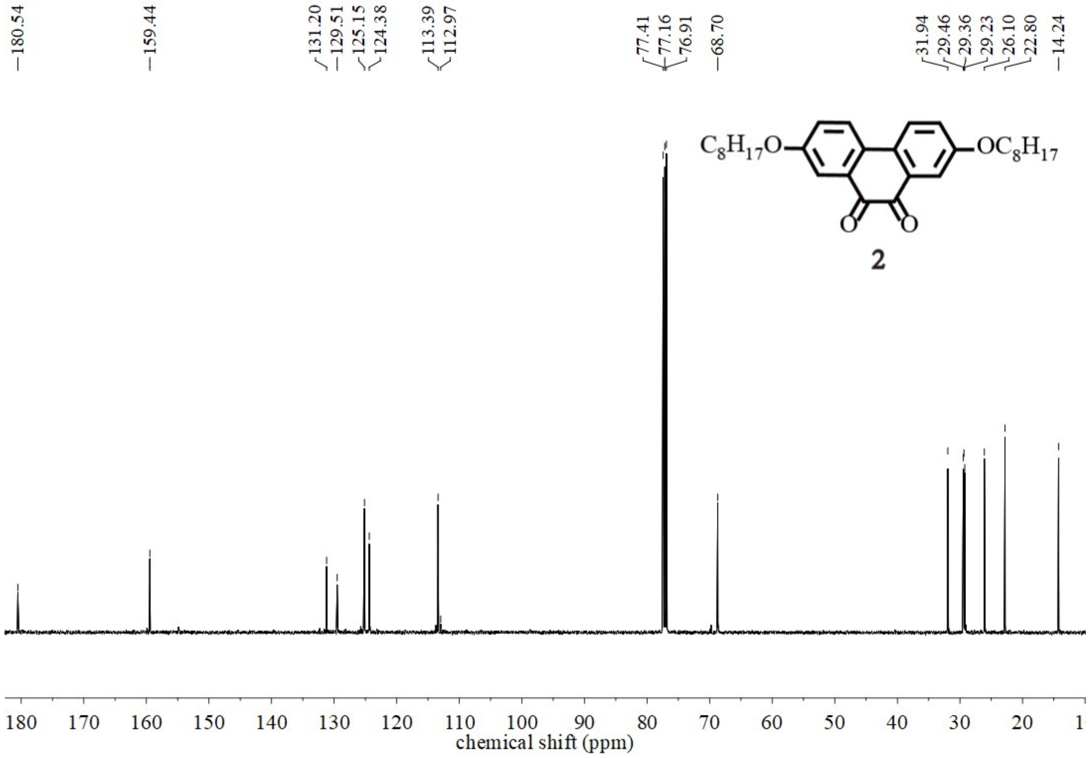

Fig. S28 ^{13}C-NMR of intermediate compound **2** (126 MHz, $CDCl_3$, r.t).

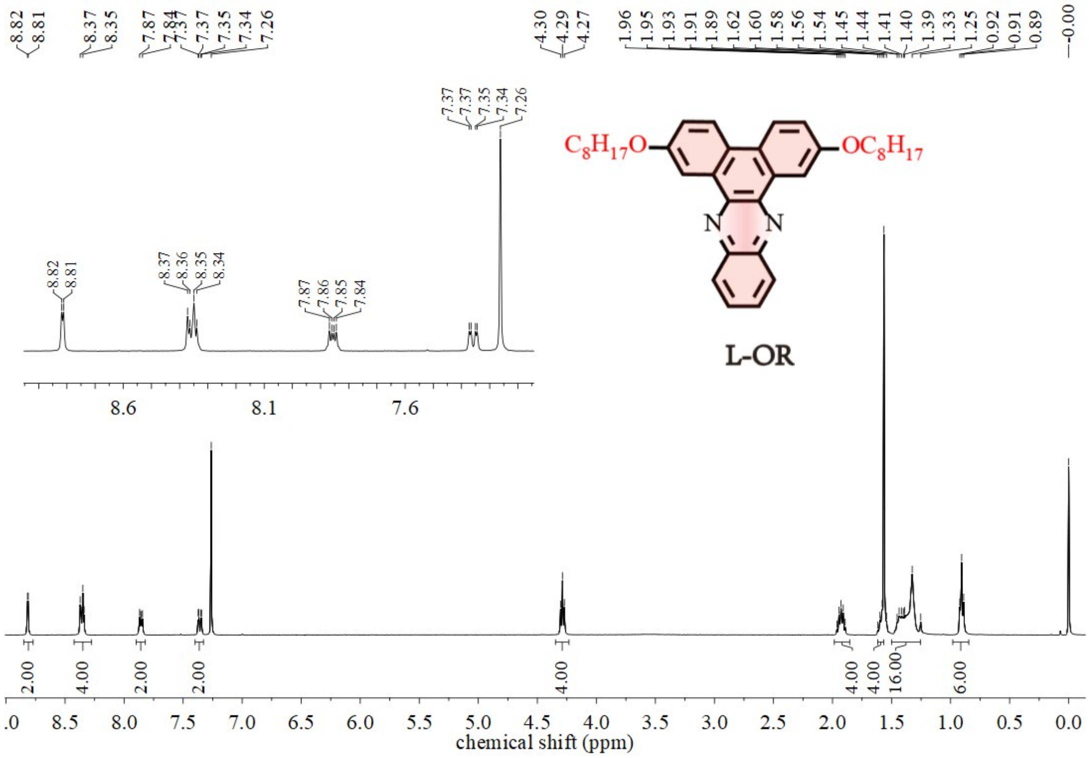

Fig. S29 ^{1}H-NMR of C^N ligand **L-OR** (400 MHz, $CDCl_3$, r.t).

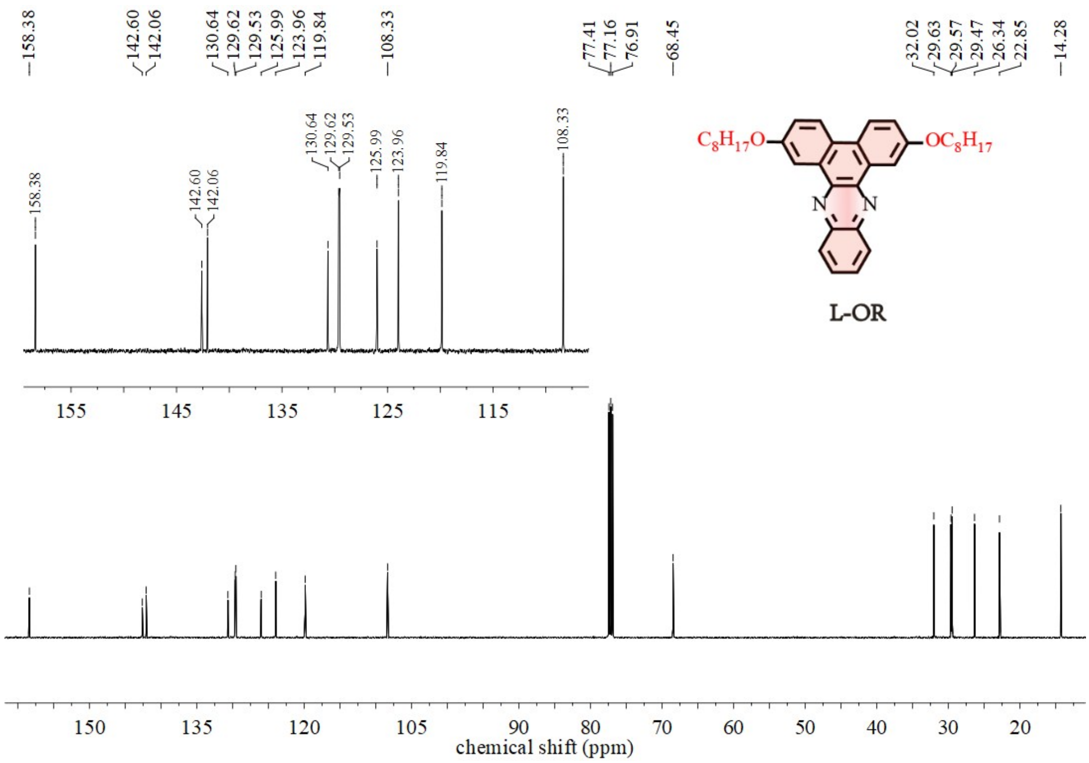

Fig. S30 ^{13}C-NMR of C^N ligand **L-OR** (126 MHz, $CDCl_3$, r.t).

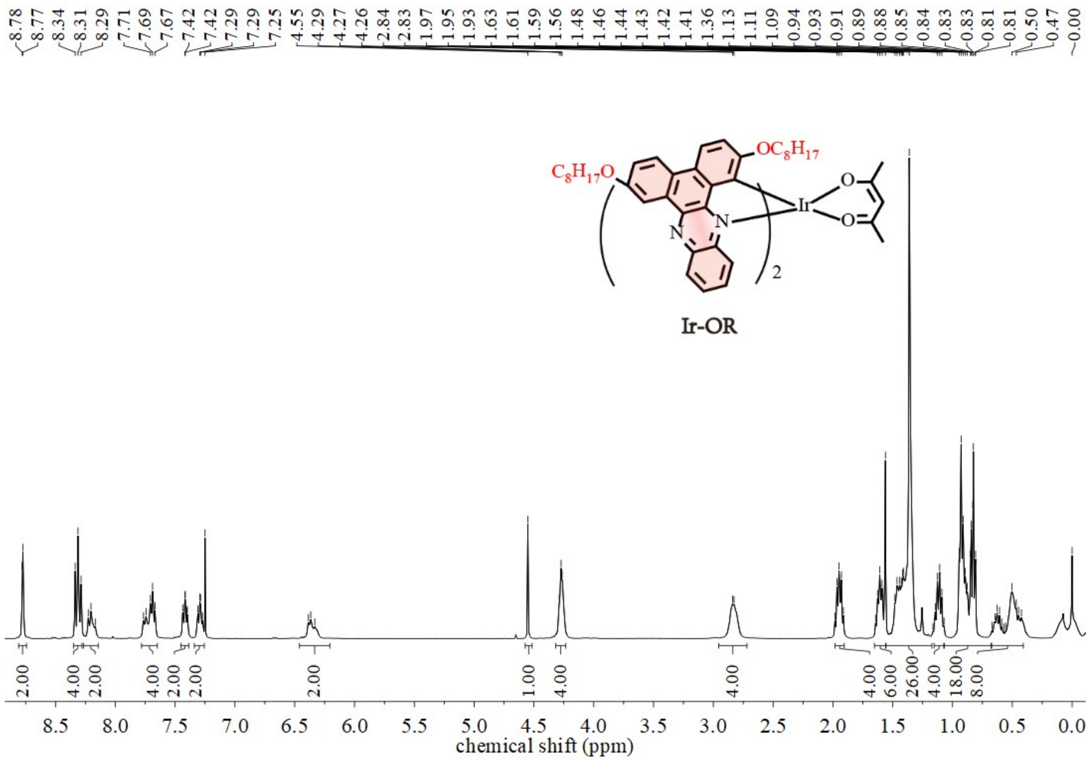

Fig. S31 ^{1}H-NMR of complex **Ir-OR** (400 MHz, $CDCl_3$, r.t).

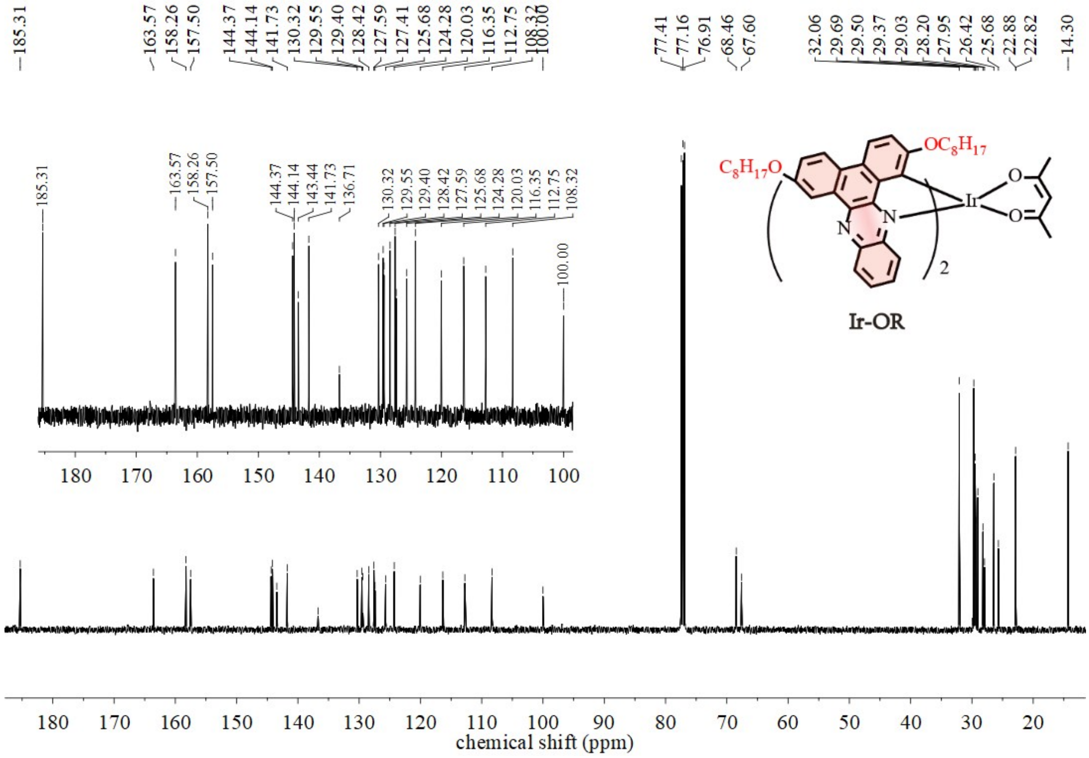

Fig. S32 ^{13}C-NMR of complex **Ir-OR** (126 MHz, $CDCl_3$, r.t).

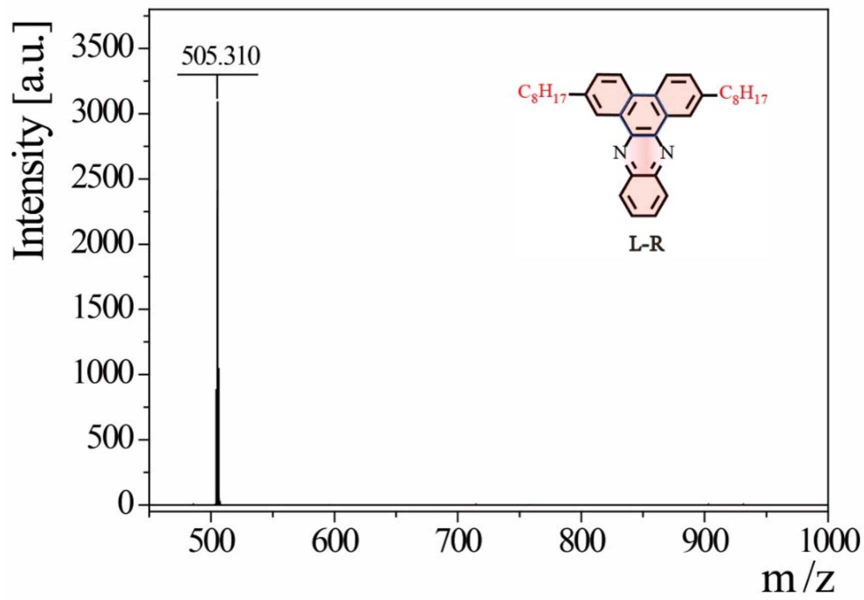

Fig. S33 MALDI-TOF-MS spectrum of C^N ligand **L-R** (CCA matrix).

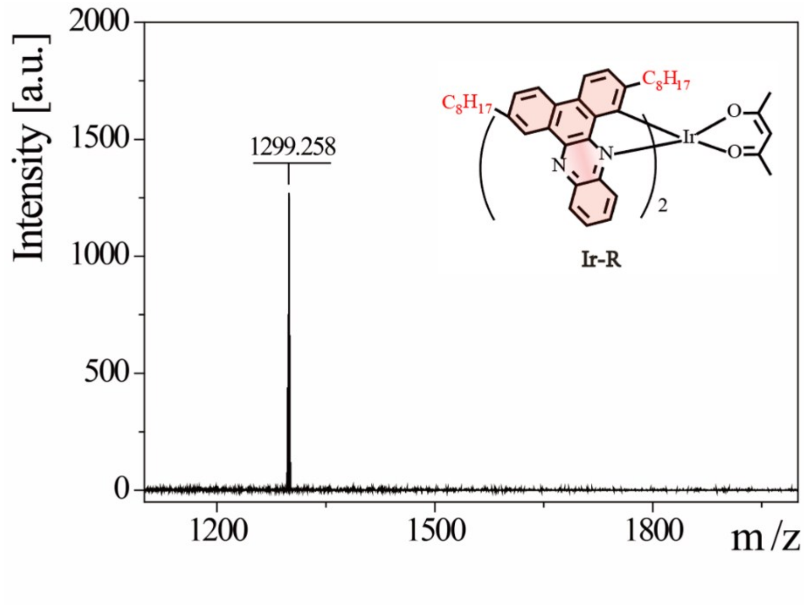

Fig. S34 MALDI-TOF-MS spectrum of complex **Ir-R** (CCA matrix).

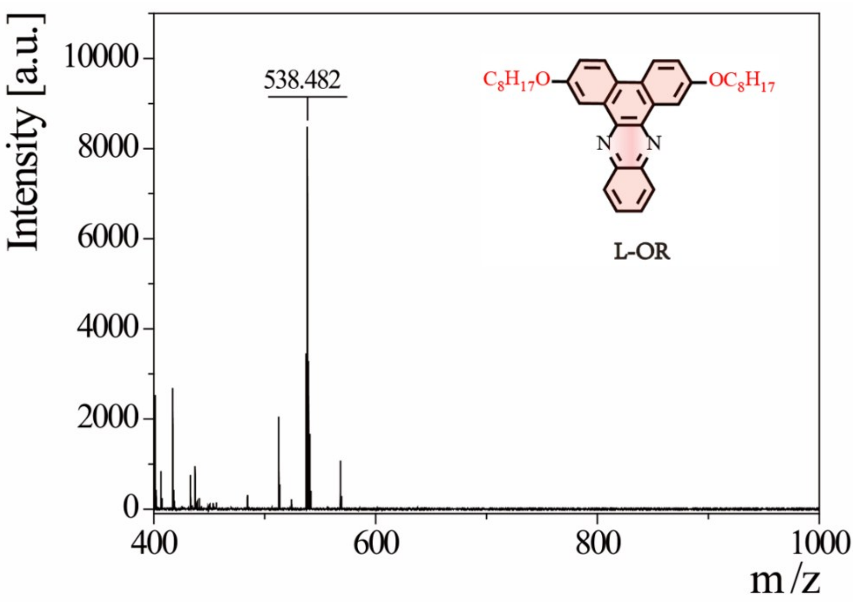

Fig. S35 MALDI-TOF-MS spectrum of C^N ligand **L-OR** (CCA matrix).

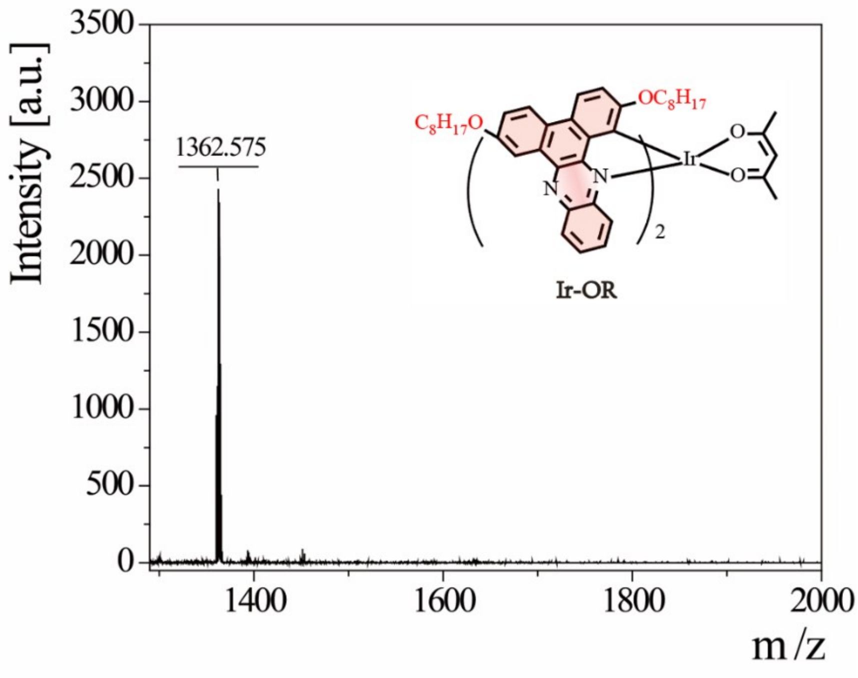

Fig. S36 MALDI-TOF-MS spectrum of complex **Ir-OR** (CCA matrix).

Table S1. Crystal data and structure refinement for complex **Ir-OR**

Empirical formula	$C_{77}H_{93}IrN_4O_6$
Formula weight	1362.75
Temperature	176.57 K
Wavelength	1.34139 Å
Crystal system	Monoclinic
Space group	$P12_1/c1$
Unit cell dimensions	a = 21.071(2) Å α= 90°. b = 22.561(2) Å β= 98.614(5)°. c = 14.0914(13) Å γ= 90°.
Volume	6623.2(11) $Å^3$
Z	4
Density (calculated)	1.367 mg/m^3
Absorption coefficient	2.992 mm^{-1}
F(000)	2832
Crystal size	0.08 x 0.05 x 0.01 mm^3
Theta range for data collection	3.243 to 55.370°.
Index ranges	-25<=h<=25, -27<=k<=27, -17<=l<=12
Reflections collected	66349
Independent reflections	12202 [R(int) = 0.0983]
Completeness to theta = 53.594°	95.7 %
Absorption correction	Semi-empirical from equivalents
Max. and min. transmission	0.7508 and 0.4415
Refinement method	Full-matrix-block least-squares on F^2
Data / restraints / parameters	12202 / 182 / 800
Goodness-of-fit on F^2	0.966
Final R indices [I>2sigma(I)]	R1 = 0.0959, wR2 = 0.2581
R indices (all data)	R1 = 0.1708, wR2 = 0.3419
Extinction coefficient	0.00011(7)
Largest diff. peak and hole	1.330 and -1.117 e. $Å^{-3}$
CCDC number	1899207

Table S2. Excited states of complex **Ir-R** and **Ir-OR** calculated using the TD-DFT

Complex	State (E_{cal} (eV), λ_{cal} (nm)	Dominant excitations (%)	Oscillator strength (f)	Character
Ir-R	S_1 (1.94,640)	H → L (97.8)	0.0045	MLCT/ILCT
	S_2 (2.06, 601)	H → L+1 (96.4)	0.0326	MLCT/ILCT
	S_3 (2.37,524)	H-2 → L (2.6) H-1 → L (93.6)	0.1183	MLCT/ILCT
	S_4 (2.57, 483)	H-5 → L (2.4) H-1 → L+1 (91.8)	0.0009	MLCT/ILCT
	S_5 (2.69, 460)	H-3 → L+1 (3.8) H-2 → L (92.5) H-2 → L (2.3)	0.0104	MLCT/ILCT
	T_1 (1.72, 719)	H → L (94.5)	0.0000	MLCT/ILCT
	T_2 (1.85, 669)	H-4 → L (2.3) H-1 → L (8.1) H → L+1 (86.6)	0.0000	MLCT/ILCT
	T_3 (2.01, 617)	H-7 → L (7.1) H-6 → L+1 (2.5) H-5 → L+1 (2.6) H-4 → L (4.5) H-3 → L+1 (13.5) H-1 → L (57.2) H → L+1 (4.6)	0.0000	MLCT/ILCT/LE
	T_4 (2.06, 602)	H-7 → L+1 (7.8) H-6 → L (3.4) H-5 → L (4.6) H-4 → L+1 (3.3) H-3 → L (24.3) H-1 → L+1 (46.4)	0.0000	MLCT/ILCT/LE
	T_5 (2.44, 508)	H-4 → L (19.5) H-3 → L+1 (23.3) H-2 → L (22.1) H-1 → L (21.5) H → L+1 (4.6)	0.0000	MLCT/ILCT/LE
Ir-OR	S_1 (1.83,676)	H → L (97.7)	0.0029	MLCT/ILCT
	S_2 (1.91, 648)	H → L+1 (97.1)	0.0411	MLCT/ILCT
	S_3 (2.21,560)	H-1 → L (96.5)	0.0784	MLCT/ILCT
	S_4 (2.33, 532)	H-2 → L (2.9) H-1 → L+1 (94.6)	0.0015	MLCT/ILCT
	S_5 (2.56, 485)	H-3 → L (96.6)	0.0153	MLCT/ILCT
	T_1 (1.61, 768)	H-1 → L+1 (3.0) H → L (92.6)	0.0000	MLCT/ILCT
	T_2 (1.72, 721)	H-1 → L (9.0) H → L+1 (86.1)	0.0000	MLCT/ILCT

	T_3 (1.95, 637)	H-6 → L (4.2) H-4 → L (3.3) H-2 → L (4.1) H-2 → L+1 (11.3) H-1 → L (57.7) H-1 → L+1 (2.3) H → L+1 (5.5)	0.0000	MLCT/ILCT/LE
	T_4 (2.01, 617)	H-6 → L+1 (4.0) H-5 → L (3.3) H-4 → L+1 (3.1) H-3 → L+1 (2.8) H-2 → L (19.2) H-2 → L+1 (2.6) H-1 → L (3.3) H-1 → L+1 (49.7)	0.0000	MLCT/ILCT/LE
	T_5 (2.34, 530)	H-6 → L (4.8) H-5 → L+1 (5.6) H-4 → L (19.3) H-3 → L (9.2) H-2 → L (6.2) H-2 → L+1 (13.7) H-1 → L (22.8) H-1 → L+1 (2.0) H → L+1 (3.6)	0.0000	MLCT/ILCT/LE

Table S3. TD-DFT results for complexes **Ir-R** and **Ir-OR** based on their optimized S_0 geometries

complex	MOs [a]	contribution percentages of metal *dπ* orbitals, *π* orbitals and flexible chains of ligands to MOs/%			main configuration of $S_0 \rightarrow S_1$ excitation /E_{cal}/λ_{cal}/*f*/character [c]	main configuration of $S_0 \rightarrow T_1$ excitation /E_{cal}/λ_{cal}/character [c]
		Ir	C^N ligand (**Me** or **OMe** chains) [b]	acac	H → L (97.8%)	H → L (94.5%)
					1.94 eV	1.72 eV
Ir-R	L+1	5.04	94.76 (0.16)	0.20	640 nm	719 nm
	L	2.79	96.78 (0.12)	0.43	0.0045	π(**L-R**)/d_π(Ir) → π*(**L-R**)
	H	33.90	63.09 (0.18)	3.01	π(**L-R**)/d_π(Ir) → π*(**L-R**)	
	H-1	19.09	65.14 (0.98)	15.77		
Ir-OR	L+1	4.60	95.24 (0.13)	0.16	H → L (97.7%)	H → L (92.6%)
	L	3.55	96.11 (0.11)	0.34	1.83 eV	H-1 → L+1 (3.0%)
	H	25.06	72.54 (1.54)	2.40	676 nm 0.0029	1.61 eV 768 nm
	H-1	4.89	92.81 (5.60)	2.30	π(**L-OR**)/d_π(Ir) → π*(**L-OR**)	π(**L-OR**)/d_π(Ir) → π*(**L-OR**)

[a] H and L denote molecular orbitals (MO) HOMO of and LUMO, respectively; [b] data in parentheses are the contributions of the aliphatic chains to molecular orbitals; [c] E_{cal}, λ_{cal},

and *f* represent calculated excitation energies, calculated absorption wavelengths, and oscillator strength, respectively.

3. Reference

1. C. M. Cardona, W. Li, A. E. Kaifer, D. Stockdale and G. C. Bazan, *Adv. Mater*., 2011, **23**, 2367-2371.

2. J. P. Duan, P. P. Sun and C. H. Cheng, *Adv. Mater*., 2003, **15**, 224-228.

3. J. Li, P. I. Djurovich, B. D. Alleyne, M. Yousufuddin, N. N. Ho, J. C. Thomas, J. C. Peters, R. Bau and M. E. Thompson, *Inorg. Chem*., 2005, **44**, 1713-1727.

4. E. J. Foster, J. Babuin, N. Nguyen and V. E. Williams, *Chem. Commun*., 2004, 2052-2053.

5. N. Takahashi, S.-i. Kato, M. Yamaji, M. Ueno, R. Iwabuchi, Y. Shimizu, M. Nitani, Y. Ie, Y. Aso, T. Yamanobe, H. Uehara and Y. Nakamura, *J. Org. Chem*., 2017, **82**, 8882-8896.